Flow, Turbulence and Combustion manuscript No.
(will be inserted by the editor)

Three-dimensional Linear Eddy Modeling of a Turbulent Lifted Hydrogen Jet Flame in a Vitiated Co-flow

Fredrik Grøvdal · Sigurd Sannan · Jyh-Yuan Chen · Alan R. Kerstein · Terese Løvås

Received: date / Accepted: date

Abstract A new methodology for modeling and simulation of reactive flows is reported in which a 3D formulation of the Linear Eddy Model (LEM3D) is used as a post-processing tool for an initial RANS simulation. In this hybrid approach, LEM3D complements RANS with unsteadiness and small-scale resolution in a computationally efficient manner. To demonstrate the RANS-LEM3D model, the hybrid model is applied to a lifted turbulent N_2-diluted hydrogen jet flame in a vitiated co-flow of hot products from lean H_2/air combustion. In the present modeling approach, mean-flow information from RANS provides model input to LEM3D, which returns the scalar statistics needed for more accurate mixing and reaction calculations. Flame lift-off heights and flame structure are investigated

F. Grøvdal
NTNU Department of Energy and Process Engineering, NO-7034 Trondheim, Norway
E-mail: fredrik.grovdal@ntnu.no

S. Sannan
SINTEF Energy Research, NO-7465 Trondheim, Norway

J.-Y. Chen
Department of Mechanical Engineering, UC Berkeley, Berkeley, CA 94720, USA

A. R. Kerstein
72 Lomitas Road, Danville, CA 94526, USA

T. Løvås
NTNU Department of Energy and Process Engineering, NO-7034 Trondheim, Norway

in detail, along with other characteristics not available from RANS alone, such as the instantaneous and detailed species profiles and small-scale mixing.

Keywords Linear Eddy Model · Turbulent mixing · Subgrid scalar closure · Turbulent reactive flows

PACS 47.27.E- · 47.27.wj

1 Introduction

State-of-the-art simulation tools in industrial applications are mainly based on the Reynolds-Averaged Navier-Stokes (RANS) equations, and hence lack the spatial and temporal resolution provided by large eddy simulation (LES) or direct numerical simulation (DNS). While DNS can give detailed insight into flow structures and turbulence-flame interactions, the method is, currently and in the foreseeable future, out of reach for most practical applications. LES and RANS, however, rely on the gradient diffusion model with the counter-gradient assumption.[1] But where LES models the smallest scales (generally assumed to be isotropic), RANS provides no information. Small-scale resolution, however, is needed to give accurate predictions of the mixing and chemistry in turbulent combustion processes. Due to the computational cost associated with DNS and LES, alternative methods to provide small-scale resolution have been pursued in recent years. One-dimensional approaches, such as the Linear Eddy Model (LEM) [1, 2] and the One-Dimensional Turbulence (ODT) model [3], are methods that resolve all scales of turbulent reactive flows at a computationally affordable cost and with promising results [4, 5, 6]. In the present study, we employ a novel formulation called the 3-dimensional Linear Eddy Model (LEM3D) [7, 8], recently implemented with detailed chemistry, to investigate the lift-off height, the flame structure and other characteristics of a turbulent lifted hydrogen jet flame in a hot vitiated co-flow.

LEM3D is developed as a research tool, both in order to complement the capabilities of RANS or LES by resolving the flame structure and to improve predictions of turbulent reactive flows. While RANS gives no information other than the averaged field and LES makes use of a sub-grid model to get information about the small scale resolution, LEM3D makes use of the averaged mass-fluxes and turbulent flow field to emulate the behavior of turbulent eddies down to the smallest scales through stochastic events called triplet maps. The formulation is

[1] For non-reacting flows the counter gradient assumption implies that the averaged transport $\overline{\rho \mathbf{u}'' \phi''}$ of a scalar ϕ is oriented in a direction opposite to the normal gradient of the turbulent diffusion.

a 3D construction based on LEM, involving three orthogonally intersecting arrays of 1D LEM domains, and coupled so as to capture the 3D character of fluid trajectories. In the hybrid approach presented here, the averaged mass-fluxes and turbulent flow field are obtained in RANS and fed to LEM3D as model input.

The vitiated co-flow burner, used as a demonstration case in the present study, was developed at UC Berkeley and first presented by Cabra et al. [9, 10]. The burner enables studies of flame lift-off and stabilization mechanisms in an environment similar to that of a gas turbine combustor. The vitiated co-flow burner and similar experiments have been used extensively for model validation in recent years, e.g. a virtually identical experimental set-up was installed at the University of Sydney with advanced diagnostics to probe the location and structure of autoignition kernels [11], conditional analysis by Cheng et al. [12] were used to reveal the reaction zone structure in mixture fraction coordinates, and at UC Berkeley a pressurized vitiated co-flow burner was installed in 2013 for investigation of the statistical likelihood of autoignition events in the mixing region [13]. Myhrvold et al. [14] explored the sensitivity of predictions to the boundary conditions to validate the Eddy Dissipation Concept, and the DQMOM based PDF transport modeling by Lee et al. [15] was validated to indicate that the model has the capability of predicting the autoignition, the flame lift-off and the stabilization process.

The hot co-flow of the vitiated co-flow burner consists of combustion products from lean premixed hydrogen-air flames, which mimics the recirculated hot combustion products in practical combustors to enhance flame stability. The advantage is that the simplified flow of the burner removes the complexity of recirculating flows and hence makes the vitiated co-flow burner attractive for numerical modeling. The characteristics of autoignition and lift-off heights of turbulent H_2/N_2 flames issuing into hot co-flows of combustion products has been extensively studied by, e.g., Masri et al. [16] and Cao et al. [17] using PDF calculations. Myhrvold et al. [14] conducted a series of simulations and indicated the extent to which turbulence models influence the predicted lift-off height with Magnussen's Eddy

Dissipation Concept [18]. While Cao et al. [17] indicate that the lift-off is primarily controlled by chemistry, later studies showed that the autoignition events in unsteady flames are controlled by both chemistry and turbulent mixing e.g. [19]. A 3D DNS at Sandia National Laboratories simulating a planar hydrogen jet issuing with high velocity in hot slow air [20] seemed to put an end to the original uncertainty expressed by Cabra et al. [9], that is, autoignition was identified as the dominant stabilization mechanism for a lifted hydrogen flame in a hot co-flow and thus more important than the effects of flame propagation.

This paper reports on a new methodology for combustion modelling and simulation in which LEM3D is extended to reactive flows and applied to the Berkeley vitiated co-flow burner. The Berkeley burner has been selected since it is a challenging flame relevant for gas turbine applications. In Section 2 we present a summary of the Linear Eddy Model, the LEM3D formulation, and the implementation of chemistry into the model. Also, the details of the initial RANS simulation is provided. The results of the study are presented in Section 3, where scatter plots, contour plots and axial profiles of various scalar quantities are given. Some concluding remarks are contained in Section 4.

2 Numerical Model and Setup

2.1 Linear Eddy Modeling

The Linear Eddy Model developed by Kerstein [1, 2] was formulated to capture the mixing and reaction of scalars (like chemical species) in a computationally affordable manner. This is achieved by a reduced one-dimensional representation of the scalar fields, for which all relevant length and time scales are fully resolved. The basic idea is that the statistical description of the scalar fields in one dimension is representative of the scalar statistics of the real 3-dimensional flow.

To give further motivation for the concepts of LEM modeling, consider first the general transport equation for a reactive scalar ϕ, written as

$$\frac{\partial \rho\phi}{\partial t} + \frac{\partial\, \rho u_j \phi}{\partial x_j} = \frac{\partial}{\partial x_j}\left[\rho D_M \frac{\partial \phi}{\partial x_j}\right] + \rho\omega_\phi, \tag{1}$$

where ρ is the density, u_j is the velocity component in the coordinate direction x_j, D_M is the molecular diffusivity, and ω_ϕ is the chemical reaction rate. In the above equation a gradient type model is assumed for the diffusive flux (Fick's law), and the molecular diffusivity D_M is assumed to be represented by a mixture-averaged quantity.

For turbulent flows, the most common approximation is the Reynolds-averaged equation, below expressed in its most general form with Favre averaging, i.e.,

$$\frac{\partial\, \bar\rho\, \widetilde{\phi}}{\partial t} + \frac{\partial\, \bar\rho\, \widetilde{u}_j\, \widetilde{\phi}}{\partial x_j} = \frac{\partial}{\partial x_j}\left[\bar\rho\, D_M \frac{\partial \widetilde{\phi}}{\partial x_j} - \bar\rho\, \widetilde{u_j'' \phi''}\right] + \bar\rho\widetilde{\omega}_\phi, \tag{2}$$

where $\bar\rho$ denotes the mean of ρ, $\widetilde{\phi} = \overline{\rho\phi}/\bar\rho$ is the Favre-averaged scalar field, and $u_j'' = u_j - \widetilde{u}_j$ is the fluctuation of u_j about the Favre average $\widetilde{u}_j$. The term $\partial\,(\bar\rho\,\widetilde{u}_j\,\widetilde{\phi})/\partial x_j$ gives the advective transport based on the velocity field $\widetilde{u}_j$. The primary challenge of this approach is that it treats turbulent mixing, which by nature is an advective prosess, as a diffusion term through the mass-averaged scalar fluxes $\bar\rho\,\widetilde{u_j''\,\phi''} = -\bar\rho D_T \frac{\partial \widetilde{\phi}}{\partial x_j}$. This is called the gradient-diffusion assumption, where the turbulent diffusivity D_T is positive. The implication is that the scalar flux is in the opposite direction of the mean scalar gradient. In other words, the transport of a scalar is always in the direction from a region of higher mean scalar concentrations to a region of lower concentrations. However, for inhomogeneous, anisotropic or streamline turbulence this might not be the case, i.e., in these regions we could have counter-gradient diffusion which does not obey the gradient-diffusion assumption.

A unique feature of LEM is that the model in fact makes an explicit distinction between the processes of molecular and turbulent diffusion, i.e., turbulent mixing

is treated as an advective process. This feature is crucial in order to capture the dissimilar influences of these processes on the scalar mixing, and is achieved because all relevant scales of the turbulent flow is resolved. For the 1D LEM, the governing equation of scalar transport is expressed as

$$\frac{\partial \rho \phi}{\partial t} + TM = \frac{\partial}{\partial x}\left[\rho D_M \frac{\partial \phi}{\partial x}\right] + \rho \omega_\phi, \tag{3}$$

where the molecular diffusion $\frac{\partial}{\partial x}\left[\rho D_M \frac{\partial \phi}{\partial x}\right]$ and chemical reactions $\rho\omega_\phi$ are solved directly on the LEM domain, and TM denotes stochastic triplet maps (see Sec. 2.2). The stochastic stirring and diffusive mixing affect the chemical reactions and the subsequent heat release. In terms of implementation, the reactive-diffusive processes are punctuated by the stochastic triplet map events TM.

In general, there is a governing transport equation (3) for each of the scalars (species, temperature, etc.) being part of a particular reactive flow field. Thus, LEM naturally accommodates for multiple species undergoing chemical reactions. In particular, LEM takes into account effects of differential diffusion, which plays an important role in hydrogen combustion [21, 22]. A full description of the one-dimensional LEM can be found in [1, 2].

2.2 The triplet map

The triplet maps are stochastic events in LEM which represent turbulent advection (stirring). The turbulent stirring is a distinct physical mechanism governing the mixing of scalar fields. In Lagrangian terminology, the triplet maps rearrange fluid cells, represented by the computational cells of the discretized one-dimensional domain, in such a manner that scalar length scales are reduced and local gradients are magnified. This is in accordance with the effects of compressive strain in turbulent flow. These stochastic events hence emulate the effects of individual turbulent eddies on the scalar concentration fields as illustrated in Fig. 1. Note

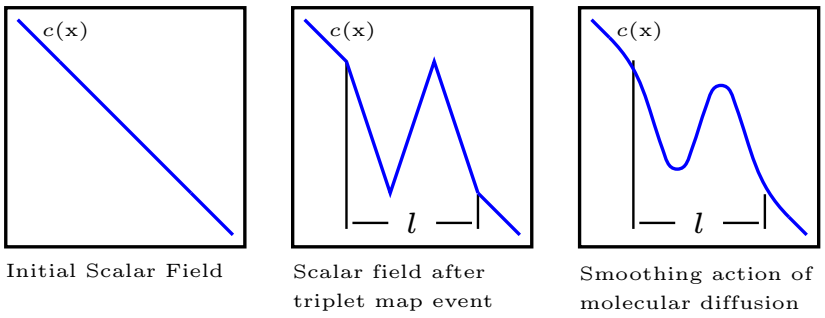

Fig. 1: Schematic diagram of a triplet mapping event of size l and the competing actions of molecular diffusion and reaction after a rearrangement event occurs.

that the effect of a single triplet map is limited to the section l, while the molecular diffusion generally affect the entire 1D domain.

2.3 LEM3D

LEM3D endeavours to maintain the distinction between chemical reactions, molecular diffusion and turbulent mixing, which means that the scalars do not mix at the molecular level by other processes than molecular diffusion. The LEM3D formulation, first described in [7, 8], incorporates three orthogonally intersecting arrays of 1D LEM domains, with intersecting LEM domains coupled in a Lagrangian sense by non-diffusive fluid-cell transfers from one domain to another (see Fig. 2). LEM3D thus provides small-scale resolution in all three spatial directions of the turbulent flow field, as well as time-resolved unsteadiness.

Diffusive time advancement takes place on each LEM domain in small sub-cycling steps within a coarser advective time step. The sub-cycling is punctuated by the randomly occurring stirring events, i.e., the triplet maps.

The coupling of the LEM domains is associated with the larger time step corresponding to the coarse-grained spatial scale defined by the intersections of orthogonal LEM domains. By construction, these intersections define a Cartesian mesh of cubic control volumes (3DCVs).

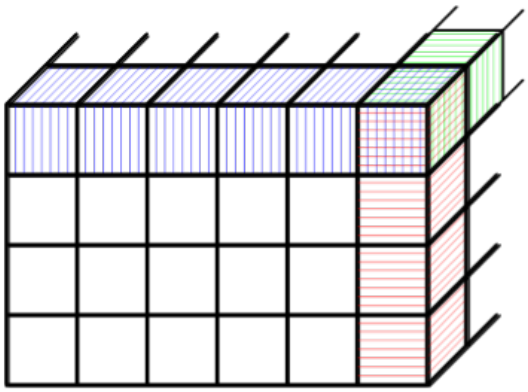

Fig. 2: The flow domain of the LEM3D simulation with the coarse Cartesian mesh consisting of 45×45×84 grid cells. The superimposed fine-scale resolution is illustrated by the coloured LEM domains in red, blue and green. One domain is shown in each coordinate direction and they intersect in the top-front corner control volume (3DCV) in LEM3D. Note that the actual LEM resolutions used in the simulations are much higher than illustrated in the figure.

The governing equation follows the structure of the stand-alone 1D LEM, but now includes the advection term, i.e.,

$$\frac{\partial\,\rho\,\phi}{\partial t}+\frac{\partial\,\bar{\rho}\,\widetilde{u}_\alpha\,\phi}{\partial x_\alpha}+TM_j=\frac{\partial}{\partial x_j}\left[\rho\,D_M\frac{\partial\phi}{\partial x_j}\right]+\rho\omega_\phi, \tag{4}$$

where the index j indicates that the terms are implemented on 1D LEM domains in three directions. Note that the conventional summation over the repeated index j is not implied for the right-hand-side term.

The averaged advection process $\partial\,(\overline{\rho}\,\widetilde{u}_\alpha\,\phi)/\partial x_\alpha$ is governed by a velocity and mean density field $\bar{\rho}$ which are prescribed from a global flow solver or measurements. The advection is implemented deterministically by Lagrangian displacements of fluid cells. This process involves the intersection and coupling of the 1D domains. The other terms of Eq. (4) are explained in Section 2.1.

2.4 Implementation of chemistry

LEM3D may be considered as a "1D-DNS" in all three directions, i.e., the model is resolved down to the Batchelor scale represented by the 1D LEM cells. Hence, the 1D cells, called *wafers*, can be considered as homogeneous reactors which implies that the chemistry is implemented directly in LEM3D. In previous work, unity Lewis number, infinitely fast chemistry, and adiabatic conditions were implemented [8]. Further, the chemistry was represented through a single conserved scalar, i.e., the mixture fraction ξ. In the current formulation, detailed and finite rate chemistry is implemented with the Li mechanism [23] and solved using the CHEMKIN II software package. The chemical source term $\rho\omega_\phi$ of Eq. (4) is solved directly through the stiff solver DVODE [24]. The individual diffusion coefficients for the different species are implemented through the mixture-averaged diffusion coefficient approach [25].

Thermal expansion, i.e., dilatation, was previously accounted for by creating new cells in integer steps when the local wafer pressure was an integer number higher than the surrounding pressure. In the new implementation this is accounted for by increasing the cell volume and performing a regridding subsequently to every diffusive-reactive time step.

It should be mentioned that a third way to account for thermal expansion was suggested and implemented by Oevermann et al. in 2008 [26]. In that approach the expansion induces a flow out of the fluid cell in an Eulerian manner. This option causes some artificial diffusion. This is also the case in the modified implementation of LEM3D, since the regridding forces fluid to cross the cell boundaries and mix with the adjacent cells.

2.5 RANS simulation

The hybrid RANS-LEM3D approach is based on an initial RANS simulation which provides mean-flow information in the form of input files to LEM3D. The 3D RANS

simulation is here performed using the ANSYS Fluent package, which solves the Reynolds-Averaged Navier-Stokes equations for the mean conservation of mass, momentum and energy, along with the k-ε turbulence model. The RANS simulation is performed on a cuboidal 85×85×120 grid using a modified k-ε model. The jet inlet is approximated by a single grid cell such that the area of the jet is preserved, i.e., the grid size Δx is given by $(\Delta x)^2 = \pi(d/2)^2$, where the jet diameter is $d = 4.57$ mm. This coarse grid might seem as a crude approximation but is chosen to demonstrate the potential of the hybrid model. Additional RANS simulations with finer grids indicated that a grid-independent solution could be attained with a Cartesian grid of the order of 10^3 more grid cells than the coarse grid. An approximate measure of the error introduced by the coarse grid is that the centerline axial mean velocity differ by about 12% on the average from the grid-independent solution, while the jet velocity half-width is about 13% wider than such a solution at the axial location of the lifted flame base at $10\,d$, as measured by Cabra et al. [9]. Nonetheless, with the focus here on method demonstration, the mean-flow information based on the coarse grid simulation is considered as sufficiently accurate.

The numerical scheme used for the RANS simulation is given in Table 1. Note that $C_{1\varepsilon}$ and $C_{2\varepsilon}$ were set in accordance with Myhrvold et al. [14] to correct for the overestimated spreading rate by the standard k-ε model.

Table 1: Numerical conditions selected for computing the H_2/N_2 jet flame in a vitiated co-flow.

Domain	Cuboid, 85×85×120
Solver	Steady state
Turbulence model	Modified k-ε with $C_\mu = 0.09$, $C_{1\varepsilon} = 1.44$, $C_{2\varepsilon} = 1.83$, $\sigma_k = 1$, $\sigma_\varepsilon = 1.3$
Turbulence-chemistry interaction	Eddy-Dissipation Concept
Discretization schemes	Standard for pressure SIMPLEC for pressure-velocity coupling Second order upwind for momentum and turbulent kinetic energy
Under-relaxation factors	Pressure= 0.3, Body forces= 0.9, Momentum= 0.7, Density= 0.9

The boundary conditions used in the computation are the same as those applied in the simulations by Cabra et al. [9] and Myhrvold et al. [14], and are detailed in Table 2.

Table 2: Flame and flow boundary conditions for the jet and the co-flow.

	Central jet	Co-flow
Volumetric flow of H_2 [L_{STP}/min]	25	225
Volumetric flow of N_2 [L_{STP}/min]	75	
Volumetric flow of air [L_{STP}/min]		2100
Temperature [K]	305	1045
Mean velocity [m/s]	107	3.5
Reynolds number	23600	18600
Diameter [m], d	0.00457	0.21
Mean mole fraction, H_2	0.2537	0.0005
Mean mole fraction, N_2	0.7427	0.7532
Mean mole fraction, O_2	0.0021	0.1474
Mean mole fraction, H_2O	0.0015	0.0989

With the given numerical scheme and the boundary and initial conditions, the RANS simulation resulted in a close-to-attached flame with a lift-off height of only $1.4\,d$. Cabra et al. [9] found, through measurements, that the actual lift-off height was $10\,d$. The OH contour was used to determine the lift-off height, where the lift-off is defined as the axial location at which the OH mass fraction first reaches 600 ppm as in [9, 10, 14]. The challenge with the turbulent lifted jet flame is the high sensitivity of the lift-off height to a variety of factors, such as the co-flow temperature and the precise dilution level of the fuel jet. Thus, a series of RANS simulations with different combinations of the Energy Prandtl number and the turbulent Schmidt number away from the Fluent default values showed that converged flames with just about any lift-off height could be attained. Moreover, during these RANS simulations issues were encountered with respect to flame stabilization. This seemed to be due to hysteresis effects. Hysteresis on $T_{\text{co-flow}}$, V_{jet} and $y_{\text{N}_2,\,\text{jet}}$ affects the stability regimes layout, though for the vitiated co-flow burner, stability is most sensitive to $y_{\text{N}_2,\,\text{jet}}$, i.e., the dilution level. These hysteresis effects influencing the transition to the lifted condition are well known and documented [27]. However, it is reported for a lifted flame with similar conditions that the hysteresis effect will not affect the stability boundaries in the unsteady regime [13].

Since the intention here is to use the vitiated co-flow burner as a demonstration case for the hybrid RANS-LEM3D model, the original RANS simulation with the close-to-attached flame was used as input for the subsequent LEM3D simulation. One aspect of this is to test whether LEM3D with the given flow field can correct for the missing lift-off compared to the experiment. In other words, the sensitivity of the model with respect to the flow field is probed.

2.6 The hybrid RANS-LEM3D model

The hybrid model presented in this paper is based on an initial RANS simulation in the Fluent flow solver which in turn generates the necessary model input to

Table 3: LEM3D input properties

Δx	4.05×10^{-3} m
Δt	1.25×10^{-6} s
Δx_w	4.05×10^{-5} m
σ_k	0.7
Pressure	1 bar
Advective CFL # RANS	0.1
LEM resolution	100

LEM3D. The RANS model input to LEM3D is mean-flow information such as the mean mass-flux field $\rho\mathbf{u}$ and the turbulent diffusivity profile obtained from the turbulent viscosity ν_t of the flow. The mean mass-flux field field governs the advective transport of scalars in LEM3D, while the turbulent diffusivity governs the turbulent advection (stirring) by determining the rate at which turbulent eddy events occur. Both the mass-flux $\rho\mathbf{u}$ and the turbulent diffusivity typically vary in the spatial directions but are resolved only at the coarser length scale corresponding to the 3DCVs. The values of ν_t are fed to the centers of the control volumes, while face-normal components of $\mathbf{u}$ are provided to the 3DCV faces.

Other model inputs to LEM3D include local (within the control volumes) values for the integral length scale L_{int} and the Kolmogorov scale η, as well as a value for the scaling exponent p that governs the eddy-size dependence in the Kolmogorov inertial cascade range. The inputs are calculated from the k-ε model such that

$$\nu_t = C_\mu \frac{k^2}{\varepsilon}, \tag{5}$$

$$\eta = L_{\text{int}} \left(\frac{\nu_M}{\nu_t} \right)^{3/4}, \tag{6}$$

where $C_\mu = 0.09$ [28]. As in [29], the scaling exponent p is set equal to 4/3 . We here aim to demonstrate the LEM3D-Fluent coupling using a coarse steady-state RANS simulation in Fluent for which there is a one-to-one correspondence between the RANS grid cells and the 3DCVs. The LEM3D simulation domain is a cuboidal 45×45×84 grid and thus here a sub-domain of the Fluent domain.

However, a Cartesian mesh is employed in the RANS simulation whose control volumes coincide with the 3DCVs of the sub-domain. In this case, no interpolation is needed and the values of the turbulent diffusivity and the face-normal mass-flux components can be used as direct input to LEM3D. The input profiles are obtained by user-defined functions (UDFs) in Fluent which format the data in line with the proper input format for LEM3D. The LEM3D simulation is performed with the conditions presented in Table 3. The advective time advancement Δt is calculated through an inverse calculation setting the advective CFL number equal to 0.1. Note, however, that the given approach and settings are done for simplicity and that any RANS grid could be interpolated into a suitable mesh for LEM3D.

3 Results and discussion

The main objective of the present work has been to report on a new methodology for modelling and simulation of reactive flows in which a 3D formulation of the Linear Eddy Model LEM3D is used as a post-processing tool for an initial RANS simulation. In this hybrid approach, LEM3D complements RANS with unsteadiness and fine-scale resolution of scalar concentration profiles. The benefit of the hybrid model, compared to a corresponding DNS, is the huge cost saving factor of solving the reactive-diffusive equations on 1D domains, rather than in a full 3D computation. To leading order, the computational cost saving is estimated to be $\sim 10^4$ for this particular application, based on a fine-scale resolution of about 300 LEM wafers in each coordinate direction within each 3DCV. To demonstrate and fully challenge the RANS-LEM3D model, the hybrid model has here been applied to the UC Berkeley vitiated co-flow burner. The results of the study are presented in the following, with centerline scatter plots of various scalar quantities, OH contour plots in the centerline symmetry plane, and axial profiles of scalars along the centerline of the computational domain. The mixture fraction used in the result section is computed using Bilgers formula [30] based on the elemental mass fractions of the fuel and oxidizer.

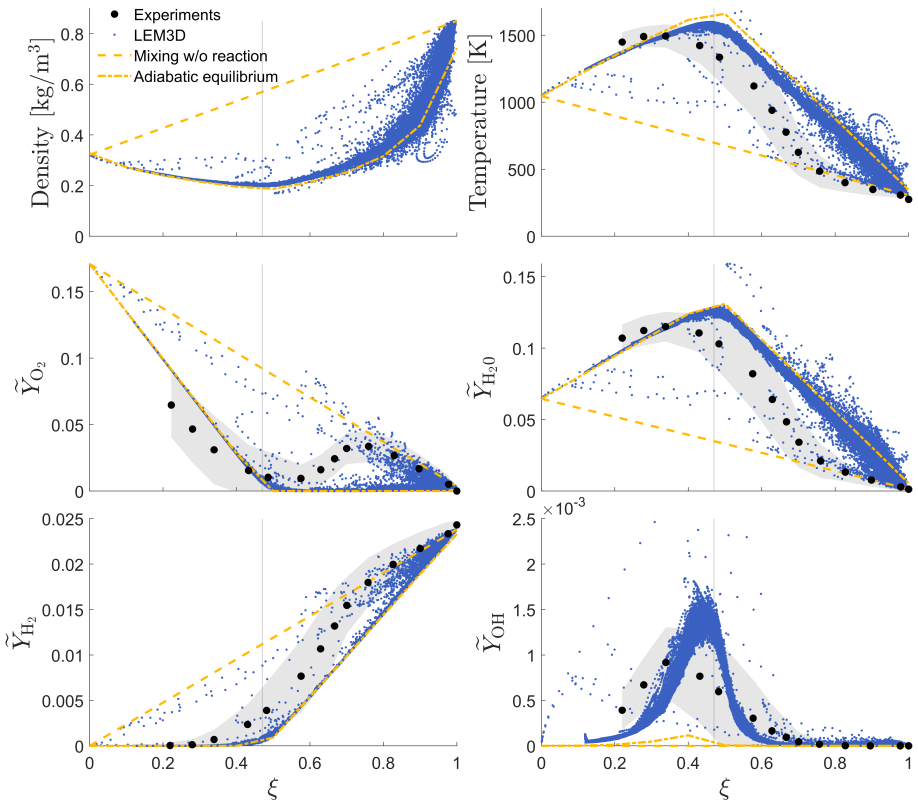

Fig. 3: Scatter plots on the centerline 1D LEM domain for various scalars versus the mixture fraction. The vertical line represents the stoichiometric mixture fraction ξ_{st}, while the gray-shaded areas represent the uncertainties of the experimental measurements [10], i.e., the variance of the scalars.

3.1 Scatter profiles

Figure 3 shows scatter plots of various scalar quantities versus the mixture fraction for the axial centerline LEM domain, together with experimental means and variances illustrated by the gray-shaded areas representing interpolated variance data taken from [10]. The dashed-dot-dashed curves represent the adiabatic equilibrium condition, computed with LOGEsoft [31] (and cross-checked with ANSYS Fluent), and the dashed curves are for mixing without reaction.

For each of the scatterplots, 41 samples are collected and plotted for the axial centerline domain, resulting in a total of 344400 points (the sum of centerline

LEM wafers sampled 41 times). The samples are collected every flow-through time after the flame has converged to a stable lift-off, and thus the scatters represent a collection of instantaneous states over the statistically steady sampling period. The scatters show reasonable agreement with the experimental curvatures, and capture both ourliers as well as more typical states. There are in some cases tendencies of a large spread, which is likely due to the largest triplet maps. This, however, is a known artifact of the model for which the very large triplet maps in some instances create too sharp gradients [7], e.g., between the fuel jet and the surrounding oxygen stream.

In comparison with the experimental results we observe that the simulation results generally lie closer to the adiabatic equilibrium lines than the measurements. Further, both for hydrogen and oxygen we observe a split in the scatters for low values of ξ, which indicates the presence of both reacting and non-reacting wafers on the centerline.

3.2 Contour plots

The flame locations of the RANS and the subsequent LEM3D simulation are illustrated in Fig. 4 through OH contours. In the plots, only the RANS/3DCV cells for which $\widetilde{Y}_{\mathrm{OH}}$ is larger than 600 ppm are shown. For LEM3D, 41 samples are collected over a time period corresponding to about 200 flow-through times.

Even though the flame stabilizes differently, both have a lift-off of approximately $1.4\,d$, based on our strict definition of lift-off height. However, by redefining the lift-off as the first appearance of the continuous contour area for which $\widetilde{Y}_{\mathrm{OH}} > 600$ ppm, we get a lift-off of about $5.9\,d$ for LEM3D. Note that LEM3D gives a flame that is a bit radially displaced outwards compared to the RANS simulation. That is, for RANS the flame is located radially at around $r/d \approx 1$, while for LEM3D it is closer to $r/d \approx 2$. We further observe that the main burning rate upstream of $z/d \approx 20$, both for RANS and LEM3D, is radially bounded by $r/d \approx 4$.

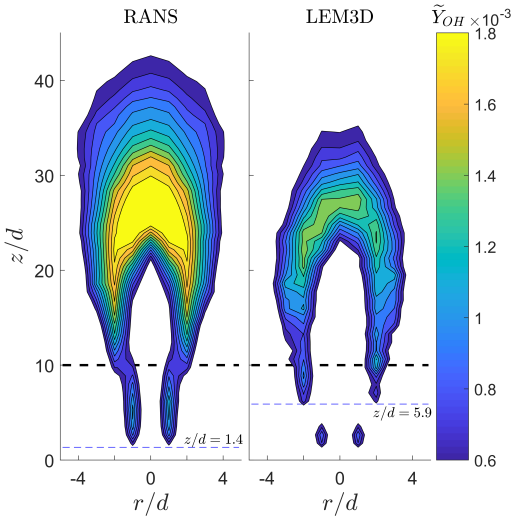

Fig. 4: Flame localization illustrated with OH contour plots of RANS versus LEM3D for the centerline symmetry plane. The black dashed line indicates the experimental lift-off $z/d = 10$, while the blue dashed lines show the computed continuous lift-off in either case.

3.3 Axial profiles

Axial profiles along the centerline for various scalars are shown in Fig. 5, together with RANS results and experimental data [9, 10]. There was no reported variance for the mixture fraction, hence no error bars are given in the ξ plot. From the mixture fraction plot, we observe that for $z/d \lesssim 25$ the co-flow fluid is reaching the centerline axial domain at a lower rate than indicated by RANS and the measurements. In general, however, the 3DCV-averaged curves are reasonably close to the data from Cabra et al. [9], except for the O_2 curve where LEM3D gives no initial peak as found in the experiment. A possible explanation for this is that the O_2 has been consumed and reacted to form H_2O in the radial domain $r/d = 2$ in LEM3D. We observe that there is H_2O at the centerline but very little O_2 upstream of $z/d \approx 25$, which indicates the lack of intrusion of unmixed co-flow fluid.

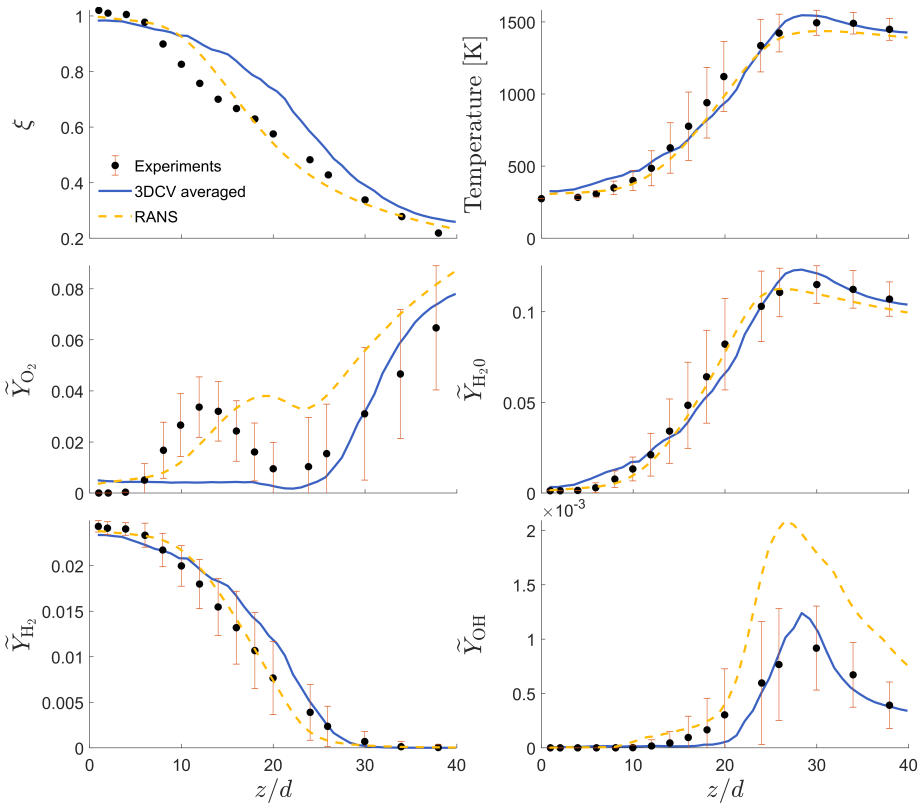

Fig. 5: Simulated axial profiles versus the measurements [9, 10] along the centerline. 3DCV averaged denotes the average value of all three LEM domains intersecting the centerline 3DCVs.

The presence of the initial O_2 peak in the measurements, and in RANS, is most likely either due to unmixed co-flow fluid reaching the centerline or to slow chemistry caused by the low temperature at the centerline. It is, however, reasonable to assume that the unreacted O_2 is due to incomplete mixing rather than to slow chemistry. Otherwise, since LEM3D is running the same chemistry as RANS, unreacted O_2 should also have shown up at the centerline in that simulation. This is supported by the flame stabilization plots in Fig. 4, which indicate that it would take longer for the OH to diffuse to the centerline for LEM3D. Hence, very little OH reaches the centerline before $z/d \approx 20$ since it reacts to form H_2O on the way.

In LEM3D, the first appearance of OH at the centerline is seen at $z/d \approx 20$. This is slightly later than indicated by the measurements of Cabra et al. [9] and by RANS, and is in agreement with the contour profiles of Fig. 4. Hence, this is where the chemical reactions start at the centerline and we see an increase in the gradients of both the temperature and the H_2O 3DCV-averaged curves downstream of $z/d = 20$.

4 Conclusions

The present paper reports on a new methodology for modeling and simulation of reactive flows in which LEM3D is used as a post-processing tool for an initial RANS simulation. In this hybrid modeling approach, LEM3D complements RANS with unsteadiness and small-scale resolution of scalar concentration profiles.

To demonstrate the RANS-LEM3D approach, the hybrid model is here applied to the UC Berkeley vitiated co-flow burner first presented by Cabra et al. [9, 10]. From the RANS output, LEM3D in general provides spatial and temporal information in good agreement with the experimental measurements. PDF transport methods are known to produce similar scatter plots as shown in Fig. 3, but ODT, which subsumes the capabilities of LEM, has been shown to provide better agreement with detailed DNS results than obtained using other models [32].

The turbulent lifted N_2-diluted hydrogen jet flame is challenging due to the high sensitivity of its lift-off height, hysteresis effects, and competing flame stabilization mechanisms [13, 27]. Here, a RANS solution based on the same numerical scheme and boundary conditions as employed by Myhrvold et al. [14] was used as model input to LEM3D. With the given Fluent default values of the standard k-ε model, and the modification of the parameter $C_{2\varepsilon}$ to correct for the spreading rate, the RANS simulation provided a close-to-attached flame.

The centerline axial profiles of scalars are, with the exception of the O_2 curve, generally in good agreement with the measurements by Cabra et al. [9]. The incapability of capturing the initial peak of the O_2 curve may be due to a known

model artifact in LEM that causes near-field discrepancies resulting from the instantaneous nature of the eddy events [2, 22]. However, it may also be due to inaccuracies in the input flow field due to the coarse RANS grid resolution or the fact that the initial RANS simulation provided a close-to-attached flame.

It has been noted that the flame configuration studied here is especially challenging for RANS-based modeling owing to the strong dependence of the results on the specification of RANS inputs. In such a situation, RANS-based combustion modeling is more useful for sensitivity analysis than for point prediction. In addition to the results presented here, numerous excursion cases have been run involving adjustment of both RANS and LEM3D parameters as well as variants of the LEM3D formulation. They indicate that agreement of particular outputs with the measurements improve or decline on a case-by-case basis. Nevertheless, the chosen flame configuration involves a degree of complexity such that the additional chemical detail provided by LEM3D, such as various scatter plots that are shown and statistics that are potentially extractable from them, could be useful for diagnosing the implications of particular RANS outcomes and more generally for sensitivity studies focused on identification of trends. This is the intended role of LEM3D post-processing of RANS combustion solutions. In the current work, the average LEM3D flame location given by the OH-contours does not coincide with the RANS flame location. Post-processing tools should in general coincide with the input on average, and improvements in this regard will be addressed in future work.

To conclude, the hybrid RANS-LEM3D methodology has here been demonstrated by application to the UC Berkeley vitiated co-flow burner. As a post-processing tool to RANS, LEM3D can provide additional scalar statistics and more detailed information on the flame structure and the small-scale mixing reactive flows. The advantage of the RANS-LEM3D model, compared to a DNS with a corresponding fine-scale resolution, is that the hybrid model represents a com-

putationally cost-efficient tool that can predict certain flame characteristics not available from RANS alone.

Acknowledgements This work was conducted at the Norwegian University of Science and Technology and SINTEF Energy Research, Norway. It was supported by The Research Council of Norway through the project HYCAP (233722).

Compliance with Ethical Standards

Conflict of interests The authors declare that they have no conflict of interest.

References

1. A. R. Kerstein, Linear-eddy modelling of turbulent transport. Part 6. Microstructure of diffusive scalar mixing fields, Journal of Fluid Mechanics 231 (1991) 361–394.
2. A. R. Kerstein, Linear-eddy modelling of turbulent transport. Part 7. Finite-rate chemistry and multi-stream mixing, Journal of Fluid Mechanics 240 (1992) 289–313.
3. A. R. Kerstein, One-dimensional turbulence: model formulation and application to homogeneous turbulence, shear flows, and buoyant stratified flows, Journal of Fluid Mechanics 392 (1999) 277–334.
4. N. Punati, J. C. Sutherland, A. R. Kerstein, E. R. Hawkes, J. H. Chen, An evaluation of the one-dimensional turbulence model: Comparison with direct numerical simulations of CO/H2 jets with extinction and reignition, Proc. Comb. Inst. 33 (2011) 1515–1522.
5. B. A. Sen, S. Menon, Linear eddy mixing based tabulation and artificial neural networks for large eddy simulations of turbulent flames, Combustion and Flame 157 (2010) 62–74.
6. V. Sankaran, S. Menon, Subgrid combustion modeling of 3-D premixed flames in the thin-reaction-zone regime, Proc. Comb. Inst. 30 (2005) 575–582.
7. S. Sannan, T. Weydahl, A. R. Kerstein, Stochastic simulation of scalar mixing capturing unsteadiness and small-scale structure based on mean-flow properties, Flow, Turbulence and Combustion 90 (2013) 189–216.
8. T. Weydahl, A Framework for Mixing-Reaction Closure with the Linear Eddy Model, Ph.D. thesis, NTNU Trondheim, 2010.
9. R. Cabra, T. Myhrvold, J. Chen, R. Dibble, A. Karpetis, R. Barlow, Simultaneous laser Raman-Rayleigh-Lif measurements and numerical modeling results of a lifted turbulent H2/N2 jet flame in a vitiated coflow, Proc. Comb. Inst. 29 (2002) 1881–1888.
10. R. Cabra, Turbulent Jet Flames Into a Vitiated Coflow, Ph.D. thesis, UC Berkeley, 2003.

11. R. L. Gordon, A numerical and experimental investigation of autoignition, Ph.D. thesis, University of Sydney, University of Sydney., 2008.
12. T. Cheng, J. Wehrmeyer, R. Pitz, Conditional analysis of lifted hydrogen jet diffusion flame experimental data and comparison to laminar flame solutions, Combustion and Flame 150 (2007) 340–354.
13. A. North, Experimental Investigations of Partially Premixed Hydrogen Combustion in Gas Turbine Environments, Ph.D. thesis, UC Berkeley, 2013.
14. T. Myhrvold, I. Ertesvåg, I. Gran, R. Cabra, J.-Y. Chen, A numerical investigation of a lifted H2/N2 turbulent jet flame in a vitiated coflow, Combustion Science and Technology 178 (2006) 1001–1030.
15. J. Lee, Y. Kim, DQMOM based PDF transport modeling for turbulent lifted nitrogen-diluted hydrogen jet flame with autoignition, International Journal of Hydrogen Energy 37 (2012) 18498–18508.
16. A. Masri, R. Cao, S. Pope, G. Goldin, PDF calculations of turbulent lifted flames of H2/N2 fuel issuing into a vitiated co-flow, Combustion Theory and Modelling 8 (2004) 1–22.
17. R. R. Cao, S. B. Pope, A. R. Masri, Turbulent lifted flames in a vitiated coflow investigated using joint PDF calculations, Combustion and Flame 142 (2005) 438–453.
18. B. F. Magnussen, Modeling of NOx and soot formation by the Eddy Dissipation Concept, Int. Flame Research Foundation (1989).
19. B. Johannessen, A. North, R. Dibble, T. Løvås, Experimental studies of autoignition events in unsteady hydrogen–air flames, Combustion and Flame 162 (2015) 3210–3219.
20. C. S. Yoo, R. Sankaran, J. H. Chen, Direct numerical simulation of turbulent lifted hydrogen jet flame in heated coflow.
21. R. W. Dibble, M. B. Long, Investigation of differential diffusion in turbulent jet flows using planar laser rayleigh scattering, Combustion and Flame 143 (4) (2005) 644–649.
22. S. Sannan, A. R. Kerstein, Differential molecular diffusion in a hydrogen-rich jet, Energy Procedia 86 (2016) 304–314.
23. J. Li, Z. Zhao, A. Kazakov, F. L. Dryer, An updated comprehensive kinetic model of hydrogen combustion, International journal of chemical kinetics 36 (2004) 566–575.
24. P. N. Brown, G. D. Byrne, A. C. Hindmarsh, Vode: A variable-coefficient ode solver, SIAM journal on scientific and statistical computing 10 (5) (1989) 1038–1051.
25. R. B. Bird, W. E. Stewart, E. N. Lightfoot, Transport Phenomena John Wiley & Sons, New York (1960) 413.
26. M. Oevermann, H. Schmidt, A. Kerstein, Investigation of autoignition under thermal stratification using Linear Eddy Modeling, Combustion and Flame 155 (2008) 370–379.

27. K. M. Lyons, Toward an understanding of the stabilization mechanisms of lifted turbulent jet flames: Experiments, Progress in Energy and Combustion Science 33 (2007) 211–231.
28. B. E. Launder, D. B. Spalding, The numerical computation of turbulent flows, Computer methods in applied mechanics and engineering 3 (2) (1974) 269–289.
29. H. Tennekes, J. L. Lumley, A First Course in Turbulence, MIT press, 1972.
30. R. Bilger, The structure of turbulent nonpremixed flames, Proc. Comb. Inst. 22 (1989) 475–488.
31. LOGE AB, LOGEsoft v1.4 Software Manuals, http://www.loge.se.
32. Z. Jozefik, A. R. Kerstein, H. Schmidt, S. Lyra, H. Kolla, J. H. Chen, One-dimensional turbulence modeling of a turbulent counterflow flame with comparison to DNS, Combustion and Flame 162 (2015) 2999–3015.